High refractive index change in Type A laser modification using a multi-scan approach

Laura Loi, Yannick Petit, Lionel Canioni

Research Article | Vol. 12, No. 6 / 1 Jun 2022 / Optical Materials Express 2297
Optical Materials EXPRESS

High refractive index change in Type A laser modification using a multi-scan approach

LAURA LOI,[1,*] YANNICK PETIT,[1,2] AND LIONEL CANIONI[1]

[1] Université de Bordeaux, CNRS, CEA, CELIA, UMR 5107, 351 Cours de la Liberation, 33405 Talence Cedex, France
[2] Université de Bordeaux, CNRS, ICMCB, UMR 5026, 87 avenue du Dr. A. Schweitzer, 33608 Pessac Cedex, France
[*] laura.loi@u-bordeaux.fr

Abstract: The focusing of femtosecond laser pulses is an efficient and robust way to fabricate integrated optical components in glasses. However, the induced refractive index changes are weak if compared with those obtained in lithography. Several solutions have been found to overcome such problem, the multi-scan technique being one of these. The present work implements the multi-scan approach on the femtosecond inscription of *Type A* laser modifications in high repetition rate regime. Therefore, a study on the effects of the absorption of subsequent laser pulses on the increase of the induced refractive index is conducted. As a result, the achievement of high and smooth refractive index change, up to 2×10^{-2}, in a commercial silver-glass is reported. Moreover, such high and controlled index contrast is exploited for the fabrication of low-propagation-losses and engineered waveguides exhibiting single-mode operation in the VIS-NIR range.

1. Introduction

Femtosecond (fs) laser tight focusing in dielectric media is a widely spread technique based on the nonlinear multi-photon absorption occurring in the interaction voxel, which allows for obtaining perennial material modifications for applications in several fields such as microfluidics, sensing and photonics. In the last two decades, this technique has quickly gained notoriety due to its simplicity and versatility to directly address 3D material structuring and associated optical properties in a wide range of materials, such as crystals [1,2], polymers [3] and mostly glasses [4–9].

Since the first demonstration in 1996 [10], the use of a focused fs source proved to be an efficient and robust way to fabricate waveguides and optical components for photonics circuits, whose downsizing is directly related to the amplitude of the induced refractive index change.

Three types of material modifications leading to a local change in the refractive index have been identified in glasses while performing direct laser writing (DLW) with a fs laser source: *Type I* being associated with a smooth negative or positive refractive index change, the latter allowing for waveguiding applications, while *Type II* and *Type III* correspond to nanogratings and voids creation, respectively [1,11–13]. Concerning the materials, many compositions have been investigated [5,7,8], yet silica-based glasses are the most commonly used so far.

In 2017 our group demonstrated the existence of a new type of refractive index change in silver-containing glasses [14] that is not associated to the glass matrix modifications. Indeed, this new refractive index change, denominated *Type A* from *Argentum*, is supported by the creation of photo-induced silver clusters: molecular-like structures that exhibit new chemical bonds, leading to the local increase of the polarizability, and provide new absorption bands in the UV, resulting in fluorescence emission. Type A modifications have shown to overcome the diffraction limit, allowing for the inscription down to 100 nm thin features [15]. Moreover, Type A refractive index change has proved to guide light, making it possible to fabricate optical components

#457655 https://doi.org/10.1364/OME.457655
Journal © 2022 Received 3 Mar 2022; revised 11 May 2022; accepted 17 May 2022; published 25 May 2022

Optical Materials EXPRESS

and photonic devices such as waveguides, couplers, beam splitters and refractive index sensors [16]. A comparison between Type A and Type I [17] shows that Type I modifications appear at laser fluence higher than that required for the creation of silver clusters, which is triggered after a significant number of pulses. Indeed, significant Type A refractive index change, and thus associated fluorescence, is achieved for 10^2 pulses and above.

The fs laser inscription is performed in two regimes: low repetition rate (from 1 kHz to 250 kHz range) and high pulse energy [3,6,7], or high repetition rate (above 1 MHz) and low pulse energy [18–20]; these two regimes show intrinsic differences regarding the thermal management.

In the case of low repetition range regime, the time scale between subsequent pulses is large enough to allow for thermal diffusion of the heat out of the voxel of interaction, preventing any significant effect of the thermal accumulation. The origin of the refractive index contrast between the induced modifications and the pristine glass is not fully understood, but it is clear that self-trapped excitons (STE) play a role. Indeed, STE are expected to provide the energy necessary to activate the localised rearrangement and densification of the lattice in some wide band-gap dielectrics, such as fused silica [21–24]. However, such refractive index change is low, typically up to 3×10^{-3} in fused silica.

For the case of high repetition rate, the many-pulse irradiation leads to the increase of the temperature above the glass transition temperature at the laser-matter interaction voxel, inducing the glass to locally melt and quickly quench. The rapid diffusion of the heat allows for obtaining symmetric material modifications and for achieving higher refractive index changes. However, the dimensions of such modifications are larger than that of the interaction voxel and the refractive index profile might be positive, negative or show both behaviours, depending on the writing parameters and the glass composition.

Remarkably, Type A refractive index change showed to occur in an athermal regime, despite the use of a high repetition rate laser source. Indeed, the low nonlinear absorption, typically 0.1% per pulse, leads to local temperature increase of a few tens of degrees only [15,25].

Still, the laser induced refractive index changes are weak if compared to the one obtained in lithography or in planar light-wave circuits (PLC) [26–28]. Many solutions have been found to achieve higher refractive index changes, such as X-ray preconditioning of the glass in order to generate precursors defects [24], the approach of laser inscription with frequency-doubled fs beam with low repetition rate [19], a post thermal treatment to eliminate the negative refractive index profile in high repetition rate regime [29], a multi-scan technique that proved to be efficient for both high and low repetition rates [2,8,30,31] and more recently fs laser induced band-gap shift to invert the sign of negative refractive index changes in crystals [32].

The multi-scan approach allows for enlarging the laser affected area and thus thermal affected region, leading to improve the associated refractive index contrast. The work of Lapointe et al. [2] reports on increasing the refractive index change of the multi-scan structures in the low repetition rate regime: up to 8.5×10^{-4} after 100 scans for both (355 fs) pulse duration, and from 1.4×10^{-3} to 9×10^{-3} after 500 scans in the case of short (65 fs) pulse duration. Moreover, for this last case, the refractive index shows a saturation around the highest value after hundreds of scans. At high repetition rate, the multi-scan technique in Type I modifications is sensitive to the increase of the pulse energy, which led to the formation of pearl-chained waveguides in fused silica with high propagation losses [31], proving that the thermal effects highly affect this regime.

In this work, the effect of the multi-scan approach on the type A refractive index change is studied, highlighting the importance of the athermal regime in the inscription of high refractive index change using a high repetition rate source. Moreover, this technique is exploited for the fabrication of high-contrast waveguides with low propagation losses.

Optical Materials EXPRESS

2. Experimental setup and procedure

The laser source used in the fabrication of the investigated structures is a prototype fs fiber laser at 1030 nm, operating at 9.25 MHz repetition rate, with pulse duration 400 fs and average output power 5 W. The sample is a commercial silver-containing zinc-phosphate glass from Argolight company with 8% of silver content (nominal cationic composition (mol%)-$39.0P_2O_5 - 53.8ZnO - 5.8Ag_2O - 1Ga_2O_3$). The positioning of the sample during the laser inscription is assured within a precision of 30 nm by motorized 3-axis stages from Newport (XMS100 - VP5ZA). A series of serpentine structures of $L = 50$ μm has been inscribed at a depth of 160 μm, to prevent aberrations, below the sample surface using a 20× microscope objective (Zeiss) with NA 0.75, varying the DLW parameters to create a matrix of irradiance. It should be noted that the DLW can be performed at different depths inside the glass, depending on the working distance of the microscope objective used to focalised the laser. If the laser intensity is adjusted during the motion along the z direction, the DLW of Type A modifications can be achieved from the surface of the glass till few hundreds of μm inside the sample. Moreover, Type A structures can be successfully inscribed almost over 100 μm depth with moderate geometrical variation while keeping the same DLW parameters. For each matrix the speed was varied from 10 to 100 μm/s while the irradiance was changed from 4 to 11 TW/cm^2. Moreover, each irradiance matrix was repeated *in loco* a number of times given by N scans, up to 20 repetitions.

Figure 1 reports the cases of irradiation matrices with a single scan (on the left) and 10 scans (on the right). The clusters fluorescence images have been acquired with a BX53 microscope (Olympus), using an Olympus EP50 camera and a 10× NA 0.3 microscope objective (Olympus) with excitation light at 345 nm. It can be noticed the increase of the fluorescence intensity after several repetitions due to the increase of the density of the photo-induced silver clusters. Each structure has been imaged using a 100× microscope objective (Zeiss) with NA 1.3 (used with a matching index oil $n = 1.518$) and the *SID4-Bio* device (Phasics) mounted on a Axiovert 200 M microscope from Zeiss, so as to extract the local optical difference (OPD) between the inscriptions and the pristine glass, as shown in Fig. 2(a). An example of a typical OPD profile associated to Type A modifications is reported in Fig. 2(b). Indeed, Type A structures are characterized by a positive refractive index change in the region where the silver clusters are photo-induced [14]. Each phase image has been processed in order to remove both acquisition noise and eventual glass inhomogeneity so as to obtain a flat background from the pristine glass. A quantitative measure of the refractive index change associated to the silver clusters for each combination of

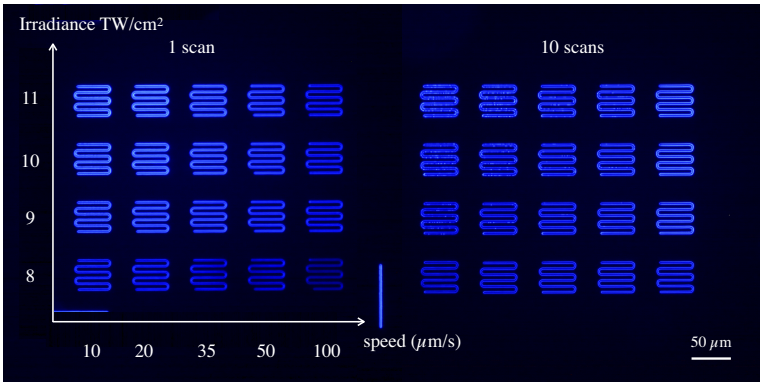

Fig. 1. Fluorescence image excited at 345 nm of two of the inscribed irradiation matrices for 1 scan (left) and 10 scans (right), respectively. For each matrix the same serpentine structure is repeated at different writing speed and laser irradiance.

Optical Materials EXPRESS

DLW parameters and number of scans is obtained by dividing the measured OPD (from Fig. 2) for the measured thickness of each structure (from Fig. 5).

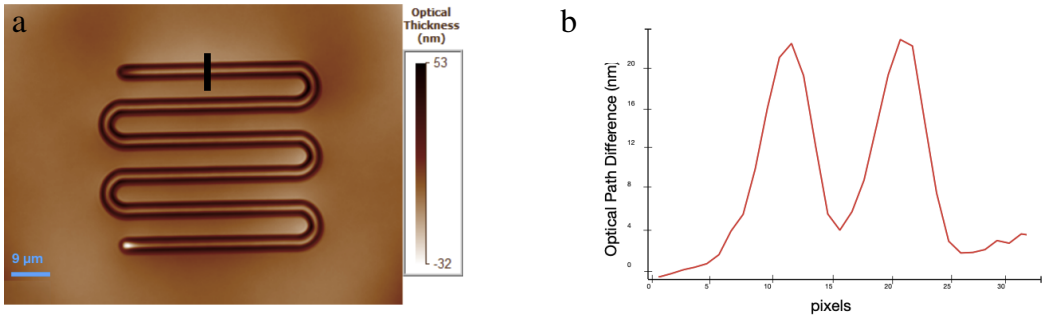

Fig. 2. (a) Example of a phase image of one serpentine laser-inscribed structure, acquired by means of the SID4-Bio device. (b) Line profile of the typical OPD associated to the double-track Type A structures. Such line profile is extracted from a vertical cross section of a single horizontal branch of the serpentine structure (along black line in (a)).

3. Results

Figure 3 reports the results of refractive index changes associated to the inscribed structures for each laser irradiance, depending on the cumulative number of pulses, *i.e.* the total number of pulses that corresponds to a given product $N\phi f_{rep}/v$ with N the number of passes and v the sample motion speed, for the given laser repetition rate f_{rep} and the typical focused beam diameter ϕ. The results in Fig. 3 show that after 0.5×10^7 pulses the refractive index contrast between the pristine glass and the photo-induced structures grows up to 1×10^{-2} for high laser irradiance, and it remarkably reaches 2×10^{-2} after 3×10^7 pulses.

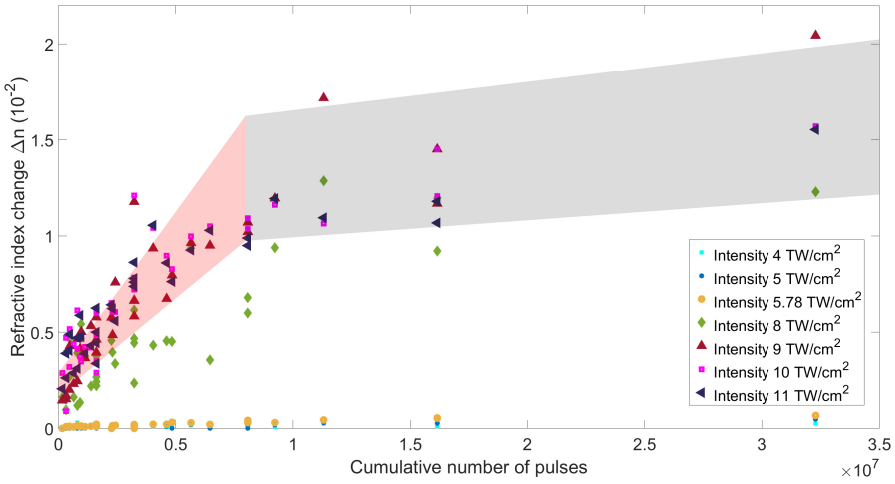

Fig. 3. Refractive index changes Δn of all the structures, inscribed with different writing parameters, with respect to the cumulative number of pulses locally irradiated during the inscription of each structure. Two different regimes are highlighted in the graph: a linear increase of Δn depending on the cumulative number of pulses (red area), proving the athermal regime; a plateau for high Δn values occurring at high number of cumulative pulses (grey area). Note that the typical error bar for each individual measure is 1.5×10^{-3}.

Optical Materials EXPRESS

Two regions have been highlighted in Fig. 3 as red and grey areas for high laser irradiances (from 8 to 11 TW/cm^2). The first region highlights a rather linear increase of the Δn with the cumulative number of pulses, which is directly related to the linear increase of the concentration of silver clusters, as a consequence of the laser inscription in an athermal regime. The second region shows the existence of a plateau, where the index contrast seems to settle on a quasi-constant value, outlining a saturation effect, as in the work of Lapointe et al. [2].

However, the saturation process in Type A inscription has a different origin. During the fs interaction of a single pulse, only a portion of the silver reservoir of the glass matrix can be exploited for the creation of silver clusters. The number of the induced clusters is directly related to the number of free electrons produced in the laser-glass interaction, thus to the laser irradiance. As a consequence, during each single pulse, part of the silver elements are getting involved in the transient trapping of holes or electrons [33]. Such temporary intermediate silver-species reservoir is thus dependent on the laser intensity. Therefore, the cumulative absorption of several pulses provides the depletion of both silver reservoirs.

The proposed description in terms of two regions for the Δn build up in Fig. 3 (shaded areas), allows for simple understanding of the cumulative management of the silver reservoir during the laser inscription. Other phenomenological modelling could have been proposed to fit the data, providing though no additional understanding at the microscopical level. Still, a phenomenological modelling would at least require to take into account the pulse-to-pulse memory effect (or incubation effects) due to local ageing process of the material, so that the phenomenological parameters shall evolve with the pulse number. A meaningful detailed modelling would require a complete numerical simulation including nonlinear energy deposition, diffusion processes, chemical reactivity, pulse-to-pulse evolution of some constants of the material as well as the management of the pulse-to-pulse distribution of silver species, as developed by Smetanina et al. [25].

Indeed, at low irradiance (from 4 to 6 TW/cm^2) the graph in Fig. 3 shows no saturation behaviour in the explored range of cumulative number of pulses. This has a two-fold meaning: on the one hand, it tells that at low and moderate laser irradiance the multi-scan technique insures a fine control of the refractive index change by simply acting on the number of cumulative absorbed pulses; on the other hand, it suggests that increasing significantly the number of pulses could lead to much higher refractive index change, potentially overcoming the results obtained so far (requiring though an undesirable longer processing time). This argumentation is corroborated by Fig. 4 that shows that the induced refractive index change is tightly dependent of the cumulative number of irradiated pulses. The four graphs in Fig. 4 represent the iso-Δn curves, *i.e.* the curves that show the same refractive index change, in the case of high laser irradiance for irradiances of 8, 9, 10 and 11 TW/cm^2. In each graph, the slope of each iso-Δn curve identifies the cumulative number of pulses necessary to achieve the labeled refractive index change. For the case of irradiances of 9, 10 and 11 TW/cm^2, the starred markers depict some of the cases in which the same refractive index change is produced thanks to the same number of cumulative pulses, but from different writing speeds and number of scans.

The selection of the DLW parameters, *i.e.* the cumulative number of pulses and the laser irradiance, targets a specific amplitude of the induced refractive index change; so, a better tuning of the latter is accomplished by adjusting the former. Thus, the results in Figs. 3 and 4 demonstrate that the management of the refractive index change of fs laser inscribed Type A structures is efficiently achieved in an athermal regime.

Optical Materials EXPRESS

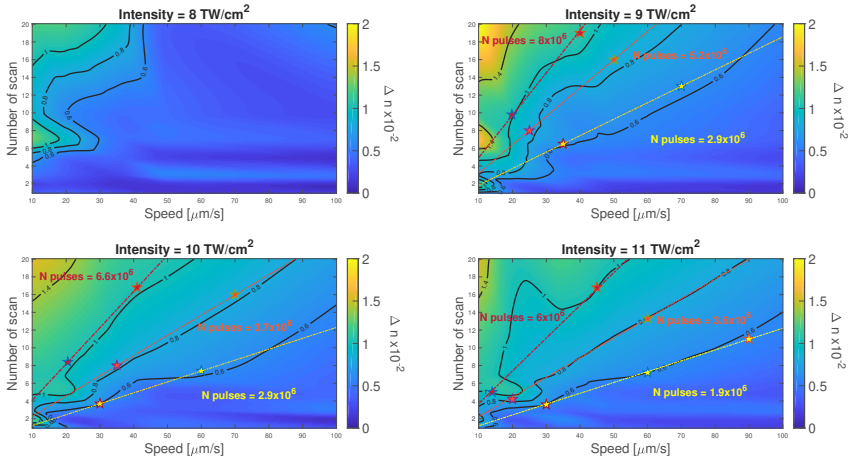

Fig. 4. Iso-Δn curves for different laser irradiances: the induced refractive index change is kept constant at the specific value along the black curves. The colored dashed lines identify for each irradiance case the slopes of such iso-curves and the starred markers highlight some cases where the cumulative number of irradiating pulses are the same although the associated writing speed and number of scans were different.

4. Functionalities

The promising results obtained in the DLW of multi-scan structures have been exploited for the fabrication of waveguides, using the above mentioned setup. The laser irradiance and the number of scanning have been chosen to be 6.2 TW/cm^2, to prevent any saturation effect, and $N_{scans} = 1, 2, 3, 5, 10, 20$ and 30, therefore realizing 7 waveguides at the writing speed of 10 μm/s. After polishing the lateral faces of the sample, the thickness of each waveguide has been imaged from side view with fluorescence and white light imaging (see Figs. 5(a) and 5(b), respectively) and measured in order to extract the corresponding refractive index change from the phase images using the SID4-Bio device and a 100× microscope objective with NA 1.3 and matching oil with $n = 1.518$. Table 1 reports on the measured values of the thickness and the width (separation between the two fluorescent tracks from top view in Fig. 5(c)) for each waveguide.

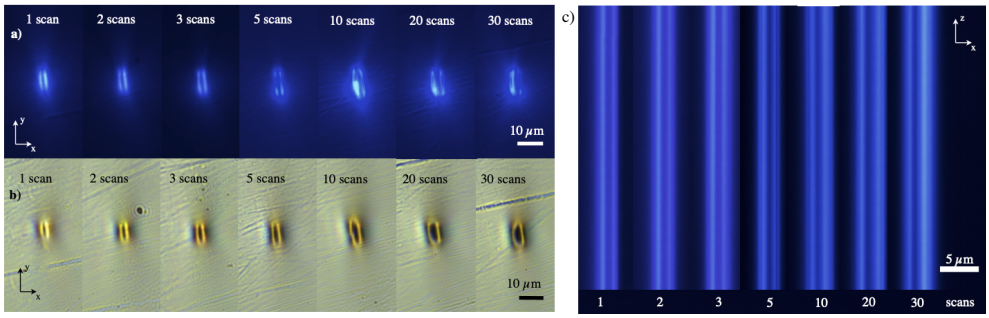

Fig. 5. (a) Fluorescence and (b) white light side-view images of the thickness of the multi-scan waveguides after polishing the lateral faces of the sample. (c) Fluorescence top-view image of the multi-scan waveguides that shows the enlarging of the width of the structures after several repetitions. Fluorescence images excited at 345 nm.

Optical Materials EXPRESS

Table 1. Measured values of thickness and width for each waveguide inscribed with different number of scans.

N scans	1	2	3	5	10	20	30
thickness (μm)	6.2	6.2	6.8	7.2	7.8	8.7	9
width (μm)	1.6	1.66	1.82	2.6	2.08	2.5	2.7

4.1. Multi-scan waveguides for improved mode confinement

The multi-scan waveguides have been injected at different wavelengths such as 750 nm, 900 nm, 1030 nm and 1550 nm, using a tunable Ti:Sapphire laser, Chameleon Ultra I (Coherent company), with a repetition rate 80 MHz, output power >2.9 W at 800 nm, and a butterfly diode laser SLD1550S-A4 (Thorlabs company), with 40 mW ASE power at 1550 nm. The injection of the Ti:Sapphire laser in the multi-scan waveguides was achieved by means of a 20× microscope objective (Olympus) with NA 0.5, while the output of the waveguides in the near field has been collected with a 100× microscope objective (Mitutoyo) with NA 0.9 and imaged on a 12 bit camera beam profiler (Thorlabs). The injection of the butterfly diode was carried out by means of a 6-axis fiber positioner (Newport), the output of the waveguides in the near field has been imaged on a 16 bit InGaAs camera (Hamammatsu). Due to the high refractive index contrast achieved with the multi-scan technique, some waveguides can support several modes beside the fundamental, as shown in Fig. 6, for wavelengths equal or shorter than 1030 nm. Higher-order modes can be excited (or inhibited) by playing on the injection position. At 1550 nm, however, all the waveguides support only the fundamental mode.

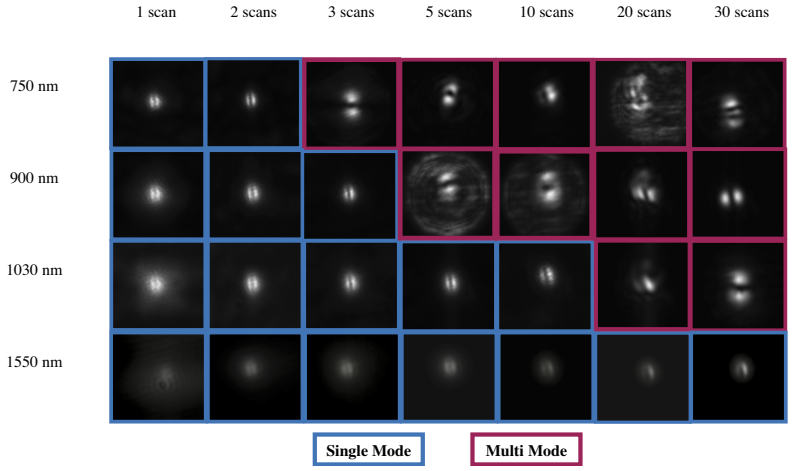

Fig. 6. Near-field images of the mode profile for each multi-scan waveguide at different wavelengths. Depending on the wavelength and number of scans at fixed speed of 10 μm/s, the waveguides can exhibit single mode or multi mode operation. Note that all the waveguides were always single mode at 1550 nm.

The near-field profiles of the waveguides have been imaged at the output face of the glass sample. As previously reported in the work of Abou Khalil et al. [14] and as shown in Fig. 7, the Type A waveguides present a peculiar mode profile due to the double-track silver-sustained structure, as a result of the photo-dissociation of the clusters in the centre of the interaction voxel during the laser inscription [15].

While being dominantly injected in the fundamental mode, the measured profiles have been processed to retrieve the Mode Field Diameters $MFD = \sqrt{<\bar{s}^2>}$ from the second statistical

Optical Materials EXPRESS

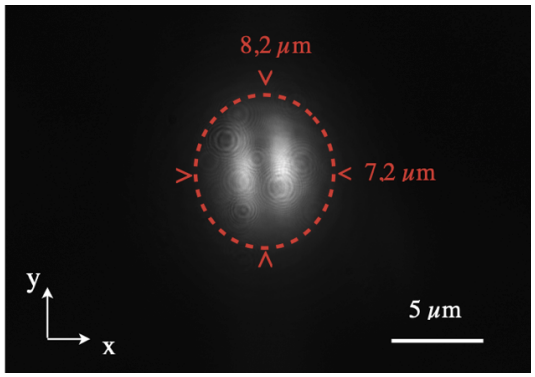

Fig. 7. Example of a processed near-field image (5 scans at 1030 nm) where the red dashed line depicts the calculated ellipse with axes on x and y equal to the Mode Field Diameters in the corresponding directions.

moment:

$$<\bar{s}^2>=\frac{\int s^2 \cdot I(s)ds}{\int I(s)ds}, \tag{1}$$

where s (either on x or y direction) is the statistical variable and I is the intensity profile along the x or y directions after having applied a binning of the 2D profile along the other direction (either y or x direction, respectively). For the case of the example reported in Fig. 7, the red dashed line depicts the equivalent astigmatic Gaussian profile with the estimated MFD along both x and y axes.

The values of the MFDs along the x and y directions are reported in Figs. 8(a) and 8(b), respectively, for each inscribed waveguide and investigated wavelengths: the two graphs show a shrinking of the mode extension along the two axes of the waveguides for increasing number of scans, as expected from the increase of the associated refractive index change.

The transmission of the waveguides has been estimated at 750 nm, 900 nm and 1030 nm in order to quantify the propagation losses, while optimising the injection by coupling the fundamental mode. The raw data from transmission measurements have been corrected by the transmission of the injecting and collecting microscope objectives, by the Fresnel losses at both the entrance and exit faces of the sample and, finally, by the coupling efficiency η at the injection, which has been estimated accordingly [34]:

$$\eta = \frac{|\int E_1^* E_2 dA|^2}{\int |E_1|^2 dA \cdot \int |E_2|^2 dA}, \tag{2}$$

where E_1^* and E_2 are the (conjugate) electric fields of the injected laser beam and the propagating fundamental mode, respectively, for each waveguide and wavelength, and the surface element dA accounts for the transverse integration over the whole profiles. The injected laser beam was directly imaged at the focus of the injection objective (while the sample had been removed) and the near-field profile of waveguided mode has been imaged at the output face of the sample. In this framework, the propagation losses at 1030 were estimated to 0.38 dB/cm for a single scan, which decreased to 0.24 dB/cm after 30 scans, as reported in Table 2.

An explanation of the decrease of the propagation losses could come from the better confinement of the guided mode on the silver-sustained structures, reducing the interaction between the mode and the pristine glass.

Optical Materials EXPRESS

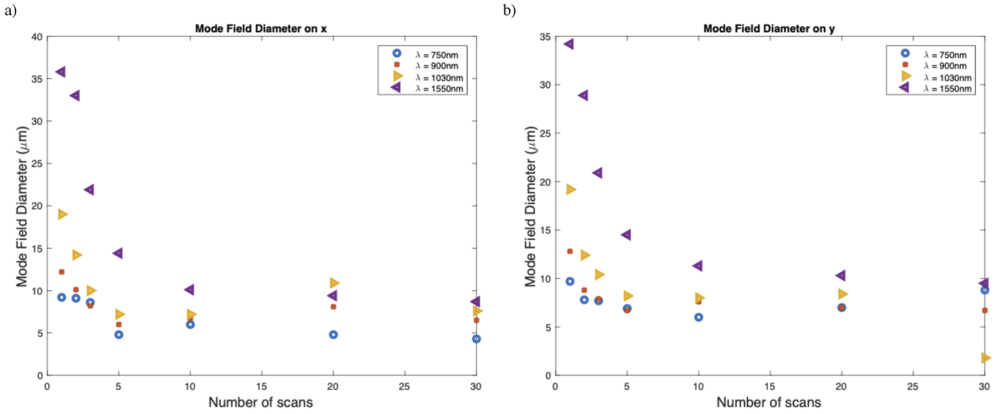

Fig. 8. Mode Field Diameters of the fundamental mode at different wavelengths: (a) x and (b) y directions, respectively. The values have been extracted from the near-field images of the modes at the output of each waveguide.

Table 2. Propagation losses for each waveguide at different wavelengths. After several scans, with the local increase of the refractive index change and associated increase of the mode confinement, the estimated propagation losses for all the wavelengths decreased by 25%, on average.

α(dB/cm)	1 scan	2 scans	3 scans	5 scans	10 scans	20 scans	30 scans
750 nm	0.35	0.33	0.41	0.5	0.34	0.29	0.26
900 nm	0.35	0.32	0.39	0.42	0.27	0.26	0.29
1030 nm	0.38	0.34	0.37	0.38	0.39	0.29	0.24

4.2. *Engineered multi-scan waveguides for Gaussian mode profile*

A multi-scan solution to retrieve a *LP*01 Gaussian profile from Type A waveguides is presented.

After a single laser scan, the beam is displaced by a distance inferior to $2\omega_0$, where ω_0 is the focused beam waist, along the direction perpendicular to the laser scan motion. During the following scan, the previously induced silver clusters will be photo-dissociated only along the track that is overlapped by the laser beam, while a new double-track is simultaneously inscribed (see Fig. 9(a)). The writing of such a new double-track is made possible thanks to remaining silver elements in the available silver reservoir, while considering low-enough laser irradiance and cumulative number of pulses, so as to prevent Type A saturation effects depicted in Fig. 3. Such multi-scan approach allows thus for the periodic inscription of individual sub-diffraction features showing inter distance below the initial double-track separation. With this inscription method of engineered multi-scan waveguides, as adopted by Liu et al. [30], it's possible to reshape the double-track waveguide into a larger structure that is able to support a gaussian-like mode.

Using the same setup, a square waveguide has been inscribed with a 6 μm thickness, made of 10 laser scans spaced by 500 nm, with an overlap of 70% between subsequent scans, so as to obtain the same width and thickness dimensions, at 100 μm/s and for a laser irradiance of 6.12 TW/cm^2.

In order to fully exploit the multi-scan technique, the reshaped waveguide was repeated 6 times *in loco* alternating the direction of the displacement, as showed in Fig. 9(a). Side-view and top-view phase images of such engineered multi-scan waveguide have been collected using a 100× microscope objective (Zeiss) with NA 1.3 and matching oil with $n = 1.518$, using the SID4-Bio (Phasics) and are reported in Figs. 9(b) and 9(c), respectively. The engineered multi-scan waveguide has been injected at 1030 nm using the same above mentioned setup; the

Optical Materials EXPRESS

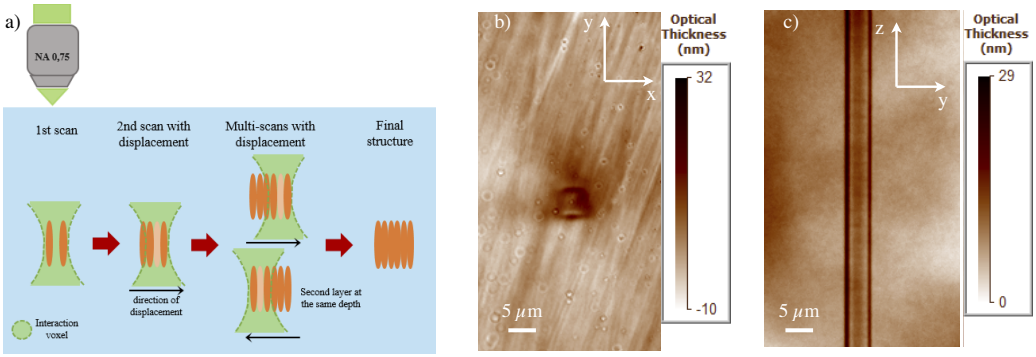

Fig. 9. (a) Schematic explanation of the procedure followed in the inscription of the engineered multi-scan waveguide. (b) Side-view and (c) top-view phase images of the reshaped waveguide. Note that the side-view image is partially affected by surface defects, contrarily to the top-view image.

guided mode has been acquired using a 16 bit Sony α III camera with no objective and it has been reported in Fig. 10, where the Gaussian profiles along the x and y directions have been highlighted respectively in blue and red.

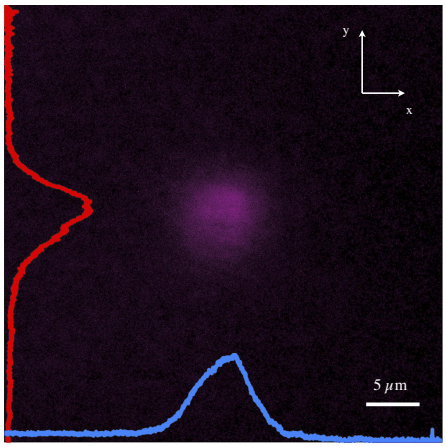

Fig. 10. Gaussian-like profile of the guided mode at 1030 nm supported by the 6 μm squared engineered multi-scan waveguide in Fig. 9.

5. Conclusion

The present work demonstrates the achievement of high refractive index change, up to 2×10^{-2}, in a commercial silver-containing glass by means of a multi-scan approach, using a high repetition rate source in a counter-intuitive athermal regime. This high refractive index contrast is supported by the photo-induced silver clusters created at each pulse and depends directly on the number of cumulative pulses absorbed during all the scans.

At high laser irradiance, the refractive index change appears to settle on a constant value after a significant amount of pulses. Such saturation effect doesn't appear for low or moderate laser irradiance, suggesting that higher refractive index contrast could be achieved by increasing significantly the number of cumulative pulses. This last task can be accomplished by either

Optical Materials EXPRESS

increasing the number of scans or by decreasing the writing speed. An interesting perspective would be to operate at higher repetition rate while considering new sources [35].

Additionally, multi-scan waveguides have been realized in order to take full advantage of such high refractive index contrast. The characterization of these waveguides showed that they can operate in single mode at different wavelenghts in the VIS-IR range, depending on the number of scans. The shrinking of the MFDs is a direct consequence of the increase of the induced refractive index change of the waveguides with respect to the surrounding pristine glass. Such a modal shrinking also led to the decrease of the associated propagation losses, from 0.38 dB/cm after a single scan down to 0.24 dB/cm after 30 scans at 1030 nm.

Finally, an engineered multi-scan solution to reshape the double-track Type A structures is presented, resulting in the achievement of a Gaussian-like LP01 mode profile. Multi-scan waveguides with high Type A refractive index change and low propagation losses can further be exploited in the fabrication of bended waveguides, enabling for miniaturization of photonic circuits.

Funding. Horizon 2020 Framework Programme (Marie Skłodowska-Curie grant agreement No 823941); Conseil Régional Nouvelle Aquitaine (APPR2020-2019-8193110); Agence Nationale de la Recherche (ANR-19-CE08-0021).

Acknowledgements. This research was funded by French National Research Agency (ANR) [Grant: **ANR-19-CE08-0021**] and Region Nouvelle Aquitaine [Grant: **APPR2020-2019-8193110**] and from European Union's Horizon 2020 research & innovation program under the Marie Skłodowska-Curie grant agreement No **823941**.

Disclosures. The authors declare no conflicts of interest.

Data Availability. Data underlying the results presented in this paper are not publicly available at this time but may be obtained from the authors upon reasonable request.

References

1. F. Chen and J. R. V. de Aldana, "Optical waveguides in crystalline dielectric materials produced by femtosecond-laser micromachining," Laser Photonics Rev. **8**(2), 251–275 (2014).
2. J. Lapointe, J.-P. Bérubé, S. Pouliot, and R. Vallée, "Control and enhancement of photo-induced refractive index modifications in fused silica," OSA Continuum **3**(10), 2851–2862 (2020).
3. J.-S. Boisvert, A. Hlil, S. Loranger, A. Riaz, Y. Ledemi, Y. Messaddeq, and R. Kashyap, "Photosensitization agents for fs laser writing in pdms," Sci. Rep. **12**(1), 1623 (2022).
4. A. M. Streltsov and N. F. Borrelli, "Study of femtosecond-laser-written waveguides in glasses," J. Opt. Soc. Am. B **19**(10), 2496–2504 (2002).
5. C. Florea and K. Winick, "Fabrication and characterization of photonic devices directly written in glass using femtosecond laser pulses," J. Lightwave Technol. **21**(1), 246–253 (2003).
6. S. Nolte, M. Will, J. Burghoff, and A. Tuennermann, "Femtosecond waveguide writing: a new avenue to three-dimensional integrated optics," Appl. Phys. A **77**(1), 109–111 (2003).
7. R. Osellame, S. Taccheo, M. Marangoni, R. Ramponi, P. Laporta, D. Polli, S. D. Silvestri, and G. Cerullo, "Femtosecond writing of active optical waveguides with astigmatically shaped beams," J. Opt. Soc. Am. B **20**(7), 1559–1567 (2003).
8. R. Martínez-Vazquez, R. Osellame, G. Cerullo, R. Ramponi, and O. Svelto, "Fabrication of photonic devices in nanostructured glasses by femtosecond laser pulses," Opt. Express **15**(20), 12628–12635 (2007).
9. R. R. Gattass and E. Mazur, "Femtosecond laser micromachining in transparent materials," Nat. Photonics **2**(4), 219–225 (2008).
10. K. M. Davis, K. Miura, N. Sugimoto, and K. Hirao, "Writing waveguides in glass with a femtosecond laser," Opt. Lett. **21**(21), 1729–1731 (1996).
11. B. Poumellec, M. Lancry, A. Chahid-Erraji, and P. G. Kazansky, "Modification thresholds in femtosecond laser processing of pure silica: review of dependencies on laser parameters," Opt. Mater. Express **1**(4), 766–782 (2011).
12. M. Will, S. Nolte, B. N. Chichkov, and A. Tünnermann, "Optical properties of waveguides fabricated in fused silica by femtosecond laser pulses," Appl. Opt. **41**(21), 4360–4364 (2002).
13. Y. Shimotsuma, P. G. Kazansky, J. Qiu, and K. Hirao, "Self-organized nanogratings in glass irradiated by ultrashort light pulses," Phys. Rev. Lett. **91**(24), 247405 (2003).
14. A. A. Khalil, J. Bérubé, S. Danto, J. Desmoulin, T. Cardinal, Y. Petit, R. Vallée, and L. Canioni, "Direct laser writing of a new type of waveguides in silver containing glasses," Sci. Rep. **7**(1), 11124 (2017).
15. M. Bellec, A. Royon, B. Bousquet, K. Bourhis, M. Treguer, T. Cardinal, M. Richardson, and L. Canioni, "Beat the diffraction limit in 3d direct laser writing in photosensitive glass," Opt. Express **17**(12), 10304–10318 (2009).
16. A. A. Khalil, P. Lalanne, J.-P. Bérubé, Y. Petit, R. Vallée, and L. Canioni, "Femtosecond laser writing of near-surface waveguides for refractive-index sensing," Opt. Express **27**(22), 31130–31143 (2019).

Optical Materials EXPRESS

17. A. A. Khalil, J.-P. Bérubé, S. Danto, T. Cardinal, Y. Petit, L. Canioni, and R. Vallée, "Comparative study between the standard type i and the type a femtosecond laser induced refractive index change in silver containing glasses," Opt. Mater. Express **9**(6), 2640–2651 (2019).
18. R. Osellame, N. Chiodo, V. Maselli, A. Yin, M. Zavelani-Rossi, G. Cerullo, P. Laporta, L. Aiello, S. D. Nicola, P. Ferraro, A. Finizio, and G. Pierattini, "Optical properties of waveguides written by a 26 mhz stretched cavity ti:sapphire femtosecond oscillator," Opt. Express **13**(2), 612–620 (2005).
19. L. Shah, A. Y. Arai, S. M. Eaton, and P. R. Herman, "Writing waveguides in glass with a femtosecond laser," Opt. Express **13**(6), 1999–2006 (2005).
20. S. Gross, N. Jovanovic, A. Sharp, M. Ireland, J. Lawrence, and M. J. Withford, "Low loss mid-infrared zblan waveguides for future astronomical applications," Opt. Express **23**(6), 7946–7956 (2015).
21. S. Mao, F. Quéré, X. Mao, R. Russo, G. Petite, and P. Martin, "Dynamics of femtosecond laser interactions with dielectrics," Appl. Phys. A **79**(7), 1695–1709 (2004).
22. D. Wortmann, M. Ramme, and J. Gottmann, "Refractive index modification using fs-laser double pulses," Opt. Express **15**(16), 10149–10153 (2007).
23. S. Richter, F. Jia, M. Heinrich, S. Döring, U. Peschel, A. Tünnermann, and S. Nolte, "The role of self-trapped excitons and defects in the formation of nanogratings in fused silica," Opt. Lett. **37**(4), 482–484 (2012).
24. M. Royon, E. Marin, S. Girard, A. Boukenter, Y. Ouerdane, and R. Stoian, "X-ray preconditioning for enhancing refractive index contrast in femtosecond laser photoinscription of embedded waveguides in pure silica," Opt. Mater. Express **9**(1), 65–74 (2019).
25. E. Smetanina, B. Chimier, Y. Petit, N. Varkentina, E. Fargin, L. Hirsch, T. Cardinal, L. Canioni, and G. Duchateau, "Modeling of cluster organization in metal-doped oxide glasses irradiated by a train of femtosecond laser pulses," Phys. Rev. A **93**(1), 013846 (2016).
26. M. Mizoshiri, Y. Hirata, J. Nishii, and H. Nishiyama, "Large refractive index changes of a chemically amplified photoresist in femtosecond laser nonlinear lithography," Opt. Express **19**(8), 7673–7679 (2011).
27. Y. Hibino, "Silica-based planar lightwave circuits and their applications," MRS Bull. **28**(5), 365–371 (2003).
28. Y. Nasu, M. Kohtoku, and Y. Hibino, "Low-loss waveguides written with a femtosecond laser for flexible interconnection in a planar light-wave circuit," Opt. Lett. **30**(7), 723–725 (2005).
29. A. Arriola, S. Gross, N. Jovanovic, N. Charles, P. G. Tuthill, S. M. Olaizola, A. Fuerbach, and M. J. Withford, "Low bend loss waveguides enable compact, efficient 3d photonic chips," Opt. Express **21**(3), 2978–2986 (2013).
30. J. Liu, Z. Zhang, C. Flueraru, X. Liu, S. Chang, and C. Grover, "Waveguide shaping and writing in fused silica using a femtosecond laser," IEEE J. Sel. Top. Quantum Electron. **10**(1), 169–173 (2004).
31. R. Graf, A. Fernandez, M. Dubov, H. Brueckner, B. Chichkov, and A. Apolonski, "Pearl-chain waveguides written at megahertz repetition rate," Appl. Phys. B **87**(1), 21–27 (2007).
32. J. Lapointe, J.-P. Bérubé, Y. Ledemi, A. Dupont, V. Fortin, Y. Messaddeq, and R. Vallée, "Nonlinear increase, invisibility, and sign inversion of a localized fs-laser-induced refractive index change in crystals and glasses," Light: Sci. Appl. **9**(1), 64 (2020).
33. Y. Petit, K. Mishchik, N. Varkentina, N. Marquestaut, A. Royon, I. Manek-Hönninger, T. Cardinal, and L. Canioni, "Dual-color control and inhibition of direct laser writing in silver-containing phosphate glasses," Opt. Lett. **40**(17), 4134–4137 (2015).
34. R. E. Wagner and W. J. Tomlinson, "Coupling efficiency of optics in single-mode fiber components," Appl. Opt. **21**(15), 2671–2688 (1982).
35. M. P. Moreno and S. S. Vianna, "Femtosecond 1 ghz ti:sapphire laser as a tool for coherent spectroscopy in atomic vapor," J. Opt. Soc. Am. B **28**(9), 2066–2069 (2011).